Anderson, A. J., Ade, P. A. R. , Ahmed, Z., Austermann, J. E., Avva, J. S., Barry, P. S., Thakur, R. Basu, Bender, A. N., Benson, B. A., Bleem, L. E., Byrum, K., Carlstrom, J. E., Carter, F. W., Cecil, T., Chang, C. L., Cho, H. M., Cliche, J. F., Crawford, T. M., Cukierman, A., Denison, E. V., de Haan, T., Ding, J., Dobbs, M. A., Dutcher, D., Everett, W., Foster, A., Gannon, R. N., Gilbert, A., Groh, J. C., Halverson, N. W., Harke-Hosemann, A. H., Harrington, N. L., Henning, J. W., Hilton, G. C., Holder, G. P., Holzapfel, W. L., Huang, N., Irwin, K. D., Jeong, O. B., Jonas, M., Khaire, T., Knox, L., Kofman, A. M., Korman, M., Kubik, D., Kuhlmann, S., Kuklev, N., Kuo, C. L., Lee, A. T., Leitch, E. M., Lowitz, A. E., Meyer, S. S., Michalik, D., Montgomery, J., Nadolski, A., Natoli, T., Nguyen, H., Noble, G. I., Novosad, V., Padin, S., Pan, Z., Pearson, J., Posada, C. M., Rahlin, A., Reichardt, C. L., Ruhl, J. E., Saunders, L. J., Sayre, J. T., Shirley, I., Shirokoff, E., Smecher, G., Sobrin, J. A., Stark, A. A., Story, K. T., Suzuki, A., Tang, Q. Y., Thompson, K. L., Tucker, C. , Vale, L. R., Vanderlinde, K., Vieira, J. D., Wang, G., Whitehorn, N., Yefremenko, V., Yoon, K. W. and Young, M. R. 2018. SPT-3G: a multichroic receiver for the South Pole Telescope. Journal of Low Temperature Physics 193 (5-6) , pp. 1057-1065. 10.1007/s10909-018-2007-z

Publishers page: http://dx.doi.org/10.1007/s10909-018-2007-z

SPT-3G: A Multichroic Receiver for the South Pole Telescope

A. J. Anderson[a,b] · P. A. R. Ade[c] · Z. Ahmed[d,e,f] · J. E. Austermann[g] ·
J. S. Avva[h] · P. S. Barry[b,i] · R. Basu Thakur[b] · A. N. Bender[j,b] ·
B. A. Benson[a,b,i] · L. E. Bleem[j,b] · K. Byrum[j] · J. E. Carlstrom[b,k,l,j,i] ·
F. W. Carter[j,b] · T. Cecil[j] · C. L. Chang[j,b,i] · H. M. Cho[f] · J. F. Cliche[m]
· T. M. Crawford[b,i] · A. Cukierman[h] · E. V. Denison[g] · T. de Haan[h] ·
J. Ding[n] · M. A. Dobbs[m,o] · D. Dutcher[b,l] · W. Everett[p] · A. Foster[q] ·
R. N. Gannon[n] · A. Gilbert[m] · J. C. Groh[h] · N. W. Halverson[p,r] ·
A. H. Harke-Hosemann[s,j] · N. L. Harrington[h] · J. W. Henning[b] · G. C. Hilton[g] ·
G. P. Holder[s,t] · W. L. Holzapfel[h] · N. Huang[h] · K. D. Irwin[d,e,f] · O. B. Jeong[h] ·
M. Jonas[a] · T. Khaire[n] · L. Knox[u] · A. M. Kofman[t,s] · M. Korman[q] ·
D. Kubik[a] · S. Kuhlmann[j] · N. Kuklev[l] · C. L. Kuo[d,e,f] · A. T. Lee[h,v] ·
E. M. Leitch[b,i] · A. E. Lowitz[b] · S. S. Meyer[b,k,l,i] · D. Michalik[w] ·
J. Montgomery[m] · A. Nadolski[s] · T. Natoli[x] · H. Nguyen[a] · G. I. Noble[m] ·
V. Novosad[n] · S. Padin[b] · Z. Pan[b,l] · J. Pearson[n] · C. M. Posada[n] · A. Rahlin[a,b]
· C. L. Reichardt[y] · J. E. Ruhl[q] · L. J. Saunders[j,b] · J. T. Sayre[p] · I. Shirley[h] ·
E. Shirokoff[b,i] · G. Smecher[z] · J. A. Sobrin[b,l] · A. A. Stark[aa] · K. T. Story[d,e] ·
A. Suzuki[h,v] · Q. Y. Tang[b,i] · K. L. Thompson[d,e,f] · C. Tucker[c] ·
L. R. Vale[g] · K. Vanderlinde[x,bb] · J. D. Vieira[s,t] · G. Wang[j] ·
N. Whitehorn[cc,h] · V. Yefremenko[j] · K. W. Yoon[d,e,f] · M. R. Young[bb]

[a]Fermi National Accelerator Laboratory, MS209, P.O. Box 500, Batavia, IL 60510-0500 · [b]Kavli Institute for Cosmological Physics, Univ. of Chicago, 5640 S. Ellis Ave., Chicago, IL 60637 · [c]School of Physics and Astronomy, Cardiff Univ., Cardiff CF24 3YB, United Kingdom · [d]Kavli Institute for Particle Astrophysics and Cosmology, Stanford Univ., 452 Lomita Mall, Stanford, CA 94305 · [e]Dept. of Physics, Stanford Univ., 382 Via Pueblo Mall, Stanford, CA 94305 ·[f]SLAC National Accelerator Laboratory, 2575 Sand Hill Rd., Menlo Park, CA 94025 · [g]National Institute of Standards and Technology, 325 Broadway, Boulder, CO 80305 · [h] Dept. of Physics, Univ. of California, Berkeley, CA 94720 · [i]Dept. of Astronomy and Astrophysics, Univ. of Chicago, 5640 S. Ellis Ave., Chicago, IL 60637 · [j]Argonne National Laboratory, High-Energy Physics Division, 9700 S. Cass Ave., Argonne, IL 60439 · [k]Enrico Fermi Institute, Univ. of Chicago, 5640 S. Ellis Ave., Chicago, IL 60637 · [l]Dept. of Physics, Univ. of Chicago, 5640 S. Ellis Ave., Chicago, IL 60637 · [m] Dept. of Physics, McGill Univ., 3600 Rue University, Montreal, Quebec H3A 2T8, Canada · [n]Argonne National Laboratory, Material Science Division, 9700 S. Cass Ave., Argonne, IL 60439 · [o]Canadian Institute for Advanced Research, CIFAR Program in Cosmology and Gravity, Toronto, ON, M5G 1Z8, Canada · [p] CASA, Dept. of Astrophysical and Planetary Sciences, Univ. of Colorado, Boulder, CO 80309 · [q]Physics Dept., Case Western Reserve Univ., Cleveland, OH 44106 · [r]Dept. of Physics, Univ. of Colorado, Boulder, CO 80309 · [s]Astronomy Dept., Univ. of Illinois, 1002 W. Green St., Urbana, IL 61801 · [t]Dept. of Physics, Univ. of Illinois, 1110 W. Green St., Urbana, IL 61801 · [u]Dept. of Physics, Univ. of California, One Shields Ave., Davis, CA 95616 · [v]Physics Division, Lawrence Berkeley National Laboratory, Berkeley, CA 94720 · [w] Univ. of Chicago, 5640 S. Ellis Ave., Chicago, IL 60637 · [x]Dunlap Institute for Astronomy and Astrophysics, Univ. of Toronto, 50 St George St, Toronto, ON, M5S 3H4, Canada · [y]School of Physics, Univ. of Melbourne, Parkville, 3010 VIC, Australia · [z]Three-Speed Logic, Inc., Vancouver, B.C., V6A 2J8, Canada · [aa]Harvard-Smithsonian Center for Astrophysics, 60 Garden St., Cambridge, MA 02138 · [bb]Dept. of Astronomy and

Abstract A new receiver for the South Pole Telescope, SPT-3G, was deployed in early 2017 to map the cosmic microwave background at 95, 150, and 220 GHz with $\sim 16,000$ detectors, 10 times more than its predecessor SPTpol. The increase in detector count is made possible by lenslet-coupled trichroic polarization-sensitive pixels fabricated at Argonne National Laboratory, new 68x frequency-domain multiplexing readout electronics, and a higher-throughput optical design. The enhanced sensitivity of SPT-3G will enable a wide range of results including constraints on primordial B-mode polarization, measurements of gravitational lensing of the CMB, and a galaxy cluster survey. Here we present an overview of the instrument and its science objectives, highlighting its measured performance and plans for the upcoming 2018 observing season.

1 Introduction

Deep, high-resolution maps of the temperature and polarization anisotropy of the cosmic microwave background (CMB) provide a wealth of cosmological information. At degree angular scales, B-mode polarization may provide direct evidence for gravitational waves produced during inflation [1, 2, 3], while the anisotropy at arcminute scales contains information about gravitational lensing of the CMB by foreground structure [4, 5] and about neutrino mass and the number of relativistic species [6]. Although arcminute-resolution CMB measurements are well-motivated, realizing significant progress on these science topics requires a large increase in sensitivity over the existing generation of receivers with $O(10^3)$ detectors, such as a SPTpol [7], ACTpol [8], and POLARBEAR [9]. The design of SPT-3G, a new receiver for the 10-m South Pole Telescope (SPT), combines a 10x increase in detector count with the excellent 1 arcmin resolution of SPT. Deployed on SPT in January 2017, the SPT-3G receiver employs trichroic pixels with $\sim 16,000$ polarization-sensitive bolometers operating in observing bands centered near 95, 150, and 220 GHz. The large number of bolometers necessitates significant changes to the optics coupling to the SPT primary, as well as a new frequency-domain multiplexing system operating at higher (68x) multiplexing factor. In this paper, we describe the scientific motivation for SPT-3G, summarize the key developments in detectors, readout, and optics that enable its advance in mapping speed, and give an overview of the current status of the instrument during its first year of observations.

2 Science Motivation

The high raw sensitivity of SPT-3G, coupled with the 1 arcmin angular resolution of the telescope, will maximize the science that can be extracted from measurements of B-mode polarization. The amplitude of primordial B-mode polarization on degree scales is parameterized by the tensor-to-scalar ratio r, and SPT-3G data on their own are forecast to achieve a 1σ sensitivity to r of 0.01 after 4 years of observing using data with multipoles greater than 50 [10]. In addition, because gravitational lensing by foreground matter converts E modes into "lensing" B modes, measuring and efficiently removing the lensing signal from B-mode maps (e.g. "delensing" [11, 12]) will become increasingly important for future constraints on r. SPT-3G can delens internally to improve the sensitivity of its own data, but

Astrophysics, Univ. of Toronto, 50 St George St, Toronto, ON, M5S 3H4, Canada · ^{cc}Dept. of Physics and Astronomy, Univ. of California, Los Angeles, CA 90095

	95 GHz	**150 GHz**	**220 GHz**
T_c **(2017)**	480-540 mK	480-540 mK	480-540 mK
P_{sat} **(2017)**	10-25 pW	12-30 pW	12-30 pW
R_n **(2017)**	1.2-2.5 Ohm	1.2-2.5 Ohm	1.2-2.5 Ohm
band center (2017)	101.2 ± 1.2 GHz	153.8 ± 1.3 GHz	223.5 ± 2.6 GHz
bandwidth (2017)	22.7 ± 0.6 GHz	37.7 ± 1.2 GHz	47.4 ± 1.8 GHz
T_c **(2018 target)**	450 mK	450 mK	450 mK
P_{sat} **(2018 target)**	10.2 pW	15.4 pW	20.0 pW
R_n **(2018 target)**	2 Ohm	2 Ohm	2 Ohm

Table 1: Summary of detector properties for wafers deployed for the 2017 observing season and targets for the wafers to be deployed for the 2018 season. Ranges given for 2017 parameters encompass the variation between wafers. Existing wafers to be deployed in 2018 have achieved significantly better consistency meeting target parameters than 2017 wafers.

its delensing power is also naturally complementary to low-resolution, small-aperture telescopes. Delensing is a strong function of resolution, and high-resolution SPT-3G data can delens observations made on the same patch of the sky by low-resolution experiments, such as BICEP/*Keck*, improving their sensitivity to *r*.

Beyond B-mode searches, the high-resolution data of SPT-3G will enable a variety of other cosmological measurements. SPT-3G will measure the lensing of the CMB, which provides an estimate of the integrated mass along the line of sight. This lensing measurement, in combination with Planck [13] and BOSS [14], will yield constraints on the sum of the neutrino masses of $\sigma(\sum m_v) = 0.06$ eV and the number of effective relativistic degrees of freedom at recombination of $\sigma(N_{eff}) = 0.06$. Neutrino mass constraints at this level will begin to constrain the inverted neutrino mass hierarchy, a scenario in which the sum of the neutrino masses is greater than 0.10 eV. SPT-3G will also find some ~ 5000 galaxy clusters at a signal-to-noise > 4.5 via the SZ effect, expanding the mass threshold and redshift range of the SPT-SZ and Planck cluster catalogs [10]. In particular, when combined with overlapping measurements from the optical Dark Energy Survey [15], the cluster measurements will enable improved constraints on dark energy and the growth of structure.

3 SPT-3G Instrument

3.1 *Focal plane*

The SPT-3G focal plane consists of $\sim 16,000$ transition-edge sensor (TES) bolometers arranged on ten 150-mm-diameter wafers containing 269 trichroic pixels each, representing a 10x increase in detector count relative to SPTpol. Multichroic pixels used in CMB experiments couple multiple sensors to a single, broadband absorber element (e.g. antenna) via filters that define frequency bands. This design increases the detector packing density in a fixed focal plane area. SPT-3G uses trichroic pixels with bands centered near 95, 150, and 220 GHz. Alumina lenslets focus light onto dual-polarization sinuous antennas, shown in Fig. 1, which are sensitive over two octaves of bandwidth [16, 17]. Signals from each polarization are split into frequency bands by three-pole quasi-lumped-element inline filters and routed to the TESs via microstrip transmission lines.

The TESs used for the 2017 observing season are Ti / Au / Ti / Au quad-layers of thickness 5 nm / 5 nm / (160-200) nm / (20-30) nm with a critical temperature (T_c) ranging from 480 mK to 540 mK, and normal impedance of 1-1.5 Ohm or 2-2.5 Ohm, depend-

ing on wafer [18, 19]. Varying the thickness of the Au layers of the TES provides control of the critical temperature [20], while the bottom 5-nm Ti layer promotes adhesion of the Au to the substrate. The variation of T_c within a wafer is < 40 mK. SPT-3G uses a three-stage ^{3}He-^{4}He sorption fridge, made by Chase Research, to cool the focal plane to a typical temperature of 280 mK in operation [21]. The saturation power of a typical deployed wafer is 17 / 22 / 25 pW for 95 / 150 / 220 GHz bolometers, but variation among the wafers spans 10-25 pW for 95 GHz bolometers, and 12-30 pW for the 150 GHz and 220 GHz bolometers. These saturation powers are generally higher than optimal, resulting in elevated readout noise-equivalent power due to the higher voltage bias required to operate the bolometers. New wafers have been fabricated for deployment in the 2017-2018 austral summer which meet saturation power targets that are $2\times$ the expected optical loading, or $P_{sat} = 10$ / 15 / 20 pW for 95 / 150 / 220 GHz bolometers [22, 23].

The combined optical efficiency of pixel, alumina lenslet, and lenslet AR coating (described in §3.3) was measured in the lab to be 60-90% for all three bands on the deployed wafers, and on-sky calibration of 95 and 150 GHz detectors using astronomical sources yield consistent efficiencies [24]. The total optical efficiency measured using astronomical sources for the 2017 season is lower than expected for the 220 GHz bolometers due to the non-optimal, two-layer antireflective (AR) coating of the alumina lenses, described in §3.3.

The yield of operable bolometers is 75.8%, with the largest sources of loss being open circuits in the cryogenic wiring (13.0%) and open TESs due to on-wafer wiring defects (6.3%). Improved assembly techniques and fabrication methods are expected to substantially improve both sources of loss in the 2018 observing season.

3.2 *Frequency-domain 68x multiplexing readout electronics*

To accommodate the larger detector count, SPT-3G uses new 68x digital frequency-domain multiplexing (DfMUX) readout electronics [25], compared with the 12x multiplexing used in SPTpol. Bolometers are biased with AC signals at frequencies between 1.6 and 5.2 MHz defined by a parallel array of inductor-capacitor-TES (LCR) resonant circuits, as shown in Fig. 2. These "LC chips" consist of components lithographed on silicon at LBNL [26], and they exhibit $> 95\%$ yield and low scatter of resonances. The dynamic range required at the SQUID for 68x multiplexing is achieved using a feedback scheme, called digital active nulling, that nulls out signals at the SQUID in a narrow bandwidth around each of the bolometer bias frequencies [27]. This screens the input inductance of the SQUID amplifiers, reducing the impedance in series with the TESs, which can degrade the voltage bias and stability. Digital active nulling is implemented using new warm electronics developed by McGill [28].

The 240 SQUID arrays fabricated by NIST [29] and deployed for the 2017 season have $> 99\%$ operational yield and excellent overall performance, but their large ~ 300 nH input inductance results in a readout noise enhancement at high bias frequencies. This occurs because the SQUID input coil and the LCR network of the bolometers form a current divider for signals injected by the nuller, so noise sources inside of the digital feedback loop (e.g. from amplifiers, digital-to-analog converters) are effectively amplified because some of the nulling current leaks "unmeasured" through the LCR network and bias resistor. SQUIDs with input inductances in the 10-50 nH range reduce the excess noise to a sub-dominant level over the full readout bandwidth. Development of low-inductance SQUIDs in collaboration with NIST and STAR Cryoelectronics is ongoing, and SQUIDs with acceptable characteristics have been tested in the lab and will be deployed for the 2018 observing season.
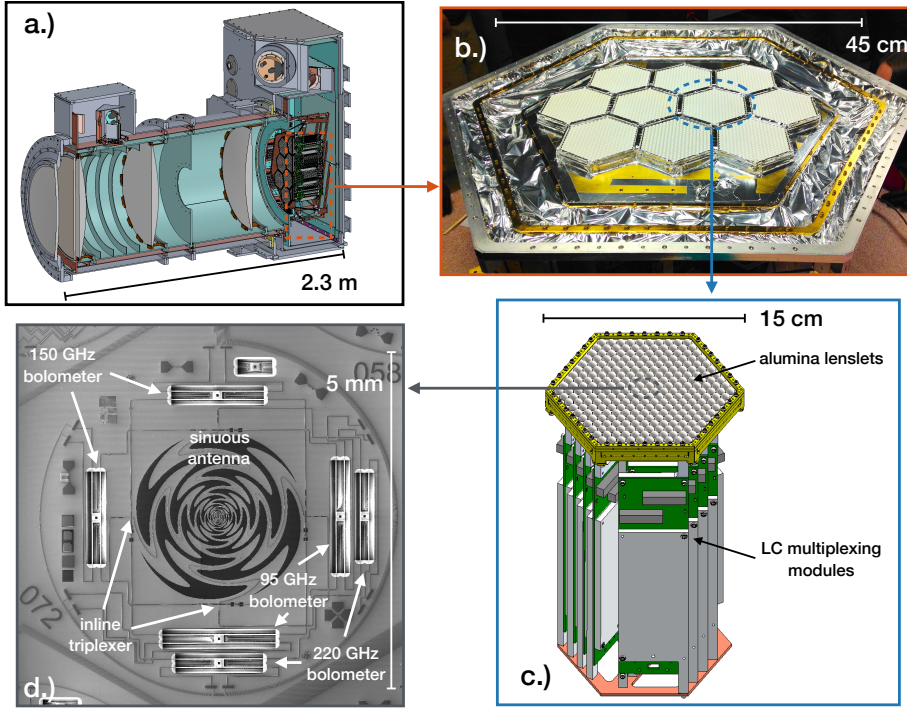
Fig. 1: *a.)* Cross-sectional drawing of cryostats containing lenses and focal plane. *b.)* Assembled focal plane of SPT-3G prior to installation on the telescope. *c.)* Detector assembly module, showing alumina lenslets, mounting hardware, and multiplexing electronics. *d.)* SPT-3G trichroic pixel, showing broadband sinuous antenna, inline triplexers that define the three observing bands, and six TES bolometers measuring three bands in two polarizations.
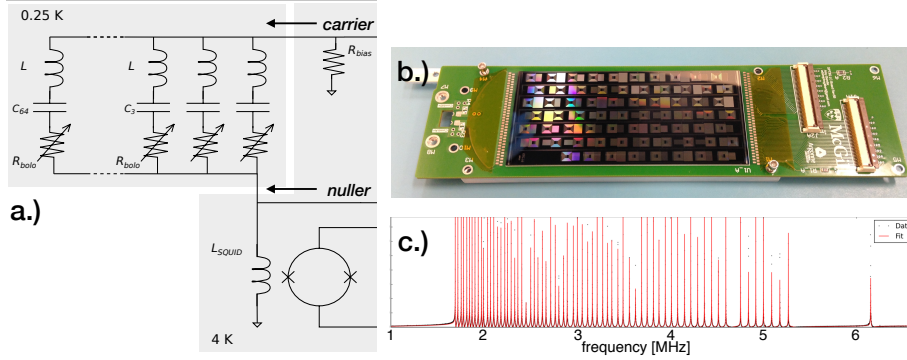

Fig. 2: *a.)* Schematic of the DfMUX system [28]. Bolometers are voltage-biased at frequencies in the range 1.6-5.2 MHz, defined by a parallel array of LCR resonators. A nuller signal produced by a digital integral feedback loop is injected before the SQUID input coil, efficiently nulling signals in a few-kHz bandwidth around the carrier tone. *b.)* LC chip with capacitors and inductors lithographed on a silicon wafer and mounted on a PCB. *c.)* Network analysis and model fit showing logarithmically-spaced resonances with excellent uniformity.

	95 GHz	150 GHz	220 GHz
$\mathbf{NET}_{bolo}$	$509\,\mu K\sqrt{s}$	$460\,\mu K\sqrt{s}$	$1188\,\mu K\sqrt{s}$
$\mathbf{NET}_{array}$	$7.4\,\mu K\sqrt{s}$	$6.5\,\mu K\sqrt{s}$	$17\,\mu K\sqrt{s}$
mapping speed ($\times$ SPTpol)	16.4	5.3	N/A

Table 2: Noise-equivalent temperature expected for the 2018 season of SPT-3G and mapping speed relative to SPTpol. Values assume deployment of three-layer plastic AR coating on all alumina surfaces, SQUIDs with ≤ 50 nH input inductance, and bolometers with saturation powers at the targets described in §3.1.

3.3 *High-throughput optical design*

SPT-3G has a 1.9 deg diameter field of view, achieved by new warm secondary optics, compared with the 1.2 deg field of view of SPTpol [30]. An ellipsoidal secondary mirror and flat tertiary mirror (both at 300 K) couple light from the primary into an optics cryostat, which consists of an HDPE window, Zotefoam filters, an alumina IR filter at 50 K, and three 720-mm diameter alumina lenses manufactured by CoorsTek at 4-5 K to reimage at the focal plane [10]. A Lyot stop at 4.5 K with a metal mesh low-pass filter reduces stray light and reduces optical loading. The 10 K secondary mirror used in SPTpol was over-illuminated such that a large fraction of the 150 GHz beam terminated on HR10 at 10 K to form an optical stop [30]. In contrast, 3G has a colder stop and under-illuminated secondary and tertiary mirrors, which results in optical power from the stop, secondary, and tertiary mirrors nearly identical to the 10K secondary of SPTpol (~ 1.1 pW). On the focal plane, hemispherical alumina lenslets are mounted on silicon wafers which are clamped on top of the detector wafers. A three-layer AR coating of PTFE and ePTFE is adhered directly to the alumina lenslets.

The use of broadband detectors and 8 large alumina surfaces (one filter and three lenses) in the optical design imposes stringent requirements on the AR coatings used in the system. The 2017 receiver deployed a suboptimal two-layer AR coating for the alumina lenses, using a plasma-sprayed mixture of alumina powder and ceramic microspheres to tune the dielectric constants [31]. For the 2018 observing season we plan to replace the two-layer coatings with a three-layer stack of PTFE and ePTFE bonded with LDPE, which has improved transmission of 99 / 99 / 98% per layer for the 95 / 150 / 220 GHz bands in simulations.

4 Status and Future Plans

During 2017, SPT-3G was used to observe a 500 deg^2 CMB field as well as astronomical sources for calibration and characterization of the instrument performance. Observing will stop in November 2017 for upgrades to the SQUIDs, AR coatings, and detector wafers, with observations of a 2500 deg^2 CMB field beginning in January 2018. Table 2 shows the array sensitivity expected during the 2018 observing season. Following the completion of a 4-year 2500 deg^2 survey, SPT-3G is projected to reach map depths in temperature of 3.6 / 3.3 / 8.5 μK arcmin at 95 / 150 / 220 GHz, which will enable measurements of CMB lensing, constraints on neutrino masses, and searches for inflationary B modes.

References

[1] U. Seljak and M. Zaldarriaga. *Phys. Rev. Lett.* 78 (1997), 2054–2057.

[2] M. Kamionkowski, A. Kosowsky, and A. Stebbins. *Phys. Rev. Lett.* 78 (1997), 2058–2061.

[3] K. N. Abazajian et al. *Astropart. Phys.* 63 (2015), 55–65.

[4] W. Hu and T. Okamoto. *Astrophys. J.* 574 (2002), 566–574.

[5] A. Lewis and A. Challinor. *Phys. Rept.* 429 (2006), 1–65.

[6] K. N. Abazajian et al. *Astropart. Phys.* 63 (2015), 66–80.

[7] A. T. Crites et al. *Astrophys. J.* 805.1 (2015), 36.

[8] R. J. Thornton et al. *Astrophys. J. Suppl.* 227.2 (2016), 21.

[9] Z. Kermish et al. *Proc. SPIE Int. Soc. Opt. Eng.* 8452 (2012), 1C.

[10] B. A. Benson et al. *Proc. SPIE Int. Soc. Opt. Eng.* 9153 (2014), 91531P.

[11] G. Simard, D. Hanson, and G. Holder. *Astrophys. J.* 807.2 (2015), 166.

[12] A. Manzotti et al. *Astrophys. J.* 846 (2017), 1.

[13] R. Adam et al. *Astron. Astrophys.* 594 (2016), A1.

[14] K. S. Dawson et al. *Astron. J.* 145 (2013), 10.

[15] B. Flaugher et al. *Astron. J.* 150 (2015), 150.

[16] R. O'Brient et al. *Appl. Phys. Lett.* 102 (2013), 063506.

[17] C. M. Posada et al. *Proc.SPIE* 9914 (2016), 9914.

[18] J. Ding et al. *IEEE Trans. Appl. Supercond.* 27.4 (2017), 2100204.

[19] W. B. Everett et al. *LTD-17* PE-10 (2017).

[20] F. W. Carter et al. *LTD-17* PC-16 (2017).

[21] R. Bhatia et al. *Cryogenics* 40.11 (2000), 685 –691. ISSN: 0011-2275.

[22] J. Ding et al. *LTD-17* PC-13 (2017).

[23] C. M. Posada et al. *LTD-17* PC-23 (2017).

[24] Z. Pan et al. *LTD-17* PA-45 (2017).

[25] J. S. Avva et al. *LTD-17* PB-18 (2017).

[26] K. Rotermund et al. *J. Low. Temp. Phys.* 184.1-2 (2016), 486–491.

[27] T. de Haan, G. Smecher, and M. Dobbs. *Proc. SPIE Int. Soc. Opt. Eng.* 8452 (2012), 84520E.

[28] A. N. Bender et al. *Proc. SPIE Int. Soc. Opt. Eng.* 9914 (2016), 99141D.

[29] M. E. Huber et al. *IEEE Trans. Appl. Supercond.* 11.1 (2001), 1251.

[30] E. M. George et al. *Proc. SPIE Int. Soc. Opt. Eng.* 8452 (2012), 84521F.

[31] O. Jeong et al. *J. Low. Temp. Phys.* 184.3-4 (2016), 621–626.